Pattern Speed of Barred Galaxies

A thesis submitted in partial fulfillment of the requirements for the award of the degree of

Master of Science

by

Pavan Vynatheya
15MS155

under

Prof. Kanak Saha, IUCAA
and
Prof. Narayan Banerjee, IISER Kolkata

to the

Department of Physical Sciences

Indian Institute of Science Education and Research, Kolkata

July 14, 2020

Declaration by the student

July 14, 2020

I, Mr. Pavan Vynatheya, Roll No. 15MS155, a student of Department of Physical Sciences of the 5 Year BS-MS Dual Degree Program of IISER Kolkata, hereby declare that this thesis is my own work and, to the best of my knowledge, it neither contains materials previously published or written by any other person, nor it has been submitted for any degree or any other academic award anywhere before. I have used the originality checking service to prevent inappropriate copying.

I also declare that all copyrighted material incorporated into this thesis is in compliance with the Indian Copyright Act, 1957 (amended in 2012) and that I have received written permission from the copyright owners for my use of their work.

I hereby grant permission to IISER Kolkata to store the thesis in a database which can be accessed by others.

Pavan Vynatheya
Department of Physical Sciences
Indian Institute of Science Education and Research Kolkata
Mohanpur 741246, West Bengal, India

Certificate from the supervisor

July 14, 2020

This is to certify that the thesis entitled *Pattern Speed of Barred Galaxies* submitted by Mr. Pavan Vynatheya, Roll No. 15MS155, a student of Department of Physical Sciences of the 5 Year BS-MS Dual Degree Program of IISER Kolkata, is based upon his own research work under my supervision. This is also to certify that neither the thesis nor any part of it has been submitted for any degree or any other academic award anywhere before. In my opinion, the thesis fulfils the requirement for the award of the degree of BS-MS.

Prof. Kanak Saha (Supervisor)
Associate Profesor
Inter-University Centre for Astronomy and Astrophysics
Pune 411007, Maharashtra, India

Prof. Narayan Banerjee (Co-supervisor)
Professor
Department of Physical Sciences
Indian Institute of Science Education and Research Kolkata
Mohanpur 741246, West Bengal, India

Acknowledgements

I thank my supervisor in IUCAA, Prof. Kanak Saha, for agreeing to let me work on this project on spiral galaxies, and guiding me through it. IUCAA was a quiet and pretty place to do a project. Dr. Soumavo Ghosh, a postdoc, was very helpful in the initial phase of my thesis. I also thank my co-supervisor in IISER Kolkata, Prof. Narayan Banerjee, for being very accomodating with the limited time I had to do my thesis.

I am thankful to my friends in IISER Kolkata, who kept in touch with me and understood the stresses involved in simultaneously doing a thesis and applying for PhD positions. More importantly, I am grateful for the time we spent talking without worries. I also thank the new friends I made at IUCAA and IISER Pune.

A new place to stay in is always challenging, and Pune was no different. However, I came to love Pune for its ambiance, climate, and connectivity. I would have liked to stay back longer, but then came coronavirus. The past few months have been rife with coronavirus-induced lockdowns and restrictions, and have been a pressing time for everyone.

A hearty thanks to my parents and sister for supporting me through the five years of my degree. During the lockdown, only my parents' pestering got me through not being lazy and completing writing my thesis.

A final thanks to the limitless world of the internet and its unending supply of entertainment and knowledge. For all its downsides, I believe that the internet has made me a better person.

Abstract

The density wave theory of the origin of spiral arms (in spiral and barred galaxies) predicts a rotational pattern speed of non-axisymmetric features, including the spiral arms and any central bar. This is the speed with which the density wave rotates around the galactic center, and thus, the angular speed of the arms themselves. However, it has been observed that the pattern speed is not constant throughout. In this thesis, we calculate the pattern speeds of the bar and the spiral arms of simulated galaxies, by using a modified version of the Tremaine-Weinberg method. We show that the spiral arms rotate slower than the bar, and that all pattern speeds decrease through time due to angular momentum transfer. We also show that the decrease in pattern speeds can be linear or exponential.

Contents

List of Figures

List of Tables

1 Introduction

1.1 Galaxies and their types

A galaxy is a gravitationally bound system of stars, stellar remnants, interstellar gas, dust, and dark matter. Galaxies are highly varied in size and shape. They can hold anywhere between a few hundred million stars to a few hundred trillion stars. There are many schemes used to classify galaxies, with the most famous being the Hubble sequence, shown in Figure 1.1. The major types of galaxies are -

- **Elliptical galaxies:** These galaxies are triaxial[1], smooth, featureless stellar systems containing negligible interstellar gas and dust. The stars in most ellipticals are old and low-mass, due to minimal star formation. The *isophotes*[2] of ellipticals are approximately concentric ellipses. In the Hubble sequence, they are characterized by their eccentricity ϵ, with E0 being nearly spherical to E7 being very elongated.

- **Spiral galaxies:** These galaxies contain a prominent axisymmetric[3] disk composed of stars, gas and dust, and a prominent central bulge. The disk contains *spiral arms* (usually two), which are sites of ongoing star formation and are brighter than the surrounding disk. Spirals can be *normal* or *barred*. In the Hubble sequence, they are characterized by the wrapping of the spiral arms, with Sa/SBa having tightly-wrapped arms and Sc/SBc having loosely-wrapped arms.

- **Lenticular galaxies:** These galaxies are intermediate between ellipticals and spirals. Like spirals, they contain a large-scale disk and a central bulge. Like ellipticals, they are smooth and featureless in appearance, with no spiral arms and negligible star formation. In the Hubble sequence, they are designated S0 and are between the Ellipticals and Spirals.

- **Irregular galaxies:** These galaxies do not have a distinct shape or structure, unlike the others. They are usually small galaxies with an abundance of gas and dust. Some Irregu-

[1] Three perpendicular axes of symmetry, like an ellipsoid

[2] Contours of constant surface brightness

[3] Cylindrical symmetry about a particular axis

lars might have been spirals or ellipticals deformed due to mergers and other gravitational forces. They are not part of the Hubble sequence due to their chaotic appearance.

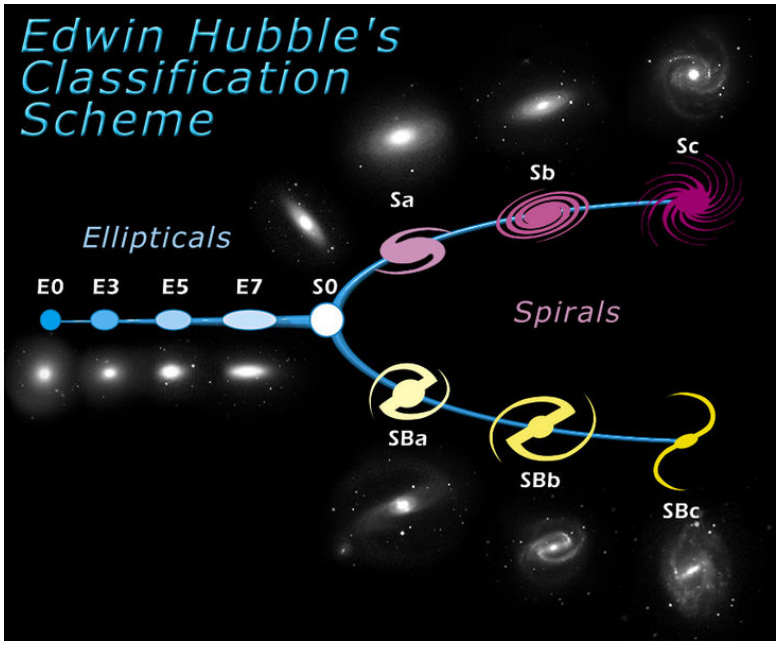

Figure 1.1: Hubble tuning-fork diagram (CosmoO)

1.2 Spiral and barred galaxies

Spiral galaxies vary in structure. *Grand spirals* have two symmetrical and very well-defined arms and *flocculent spirals* have many partial spiral arm fragments which cannot be traced to over significant angular distance. Most spiral galaxies lie in between these two extremities. Many spiral galaxies are also barred.

1.2.1 Density wave theory and pattern speed

The origin of spiral arms has always been a very intriguing mystery. Initially, they were thought to be material arms with a fixed set of stars and gas clouds. However, this results in the so-called *winding problem* due to differential rotation of stars in the galaxy. Since farther stars rotate slower, the spiral arm pattern should wind up completely in just a few orbits. Thus, material arms could not explain spiral structure.

Lin & Shu (1964) [8] formulated the *density wave theory*, a groundbreaking theory trying to explain spiral structure. They hypothesize that is that spiral structure is a *quasi-stationary*

density wave, a periodic compression and rarefaction of the disk surface density that propagates through the disk. Gravitational instabilities in the galactic disk result in the density wave. This theory states that the spiral pattern is rigid, and that there is a *pattern speed*[4] Ω_p associated with the galaxy. In the non-inertial frame rotating at Ω_p, the spiral pattern appears stationary. This does not imply that the the stars are stationary in that frame. Stars near the center of the galaxy will have angular speeds more than Ω_p, and will overtake the spiral arms as they revolve. Stars far from the center will have angular speeds less than Ω_p, and will be overtaken by the spiral arms. Calculating the pattern speed of barred galaxies is a major part of this thesis. In the next chapter, a kinematic method devised by **Tremaine & Weinberg (1984)** [21] (henceforth TW method) to calculate the pattern speed is discussed in detail.

This theory also explains why spiral arms are filled with bright, young stars. The compression of the density wave corresponds to regions of star formation - the spiral arms. Since massive stars are short-lived, they are observed very close to the arms, making them prominent. Less massive and older stars are observed throughout the galaxy. However, the Lin-Shu hypothesis is not without faults. Pattern speeds are not constant, and the spiral structure is not rigid. **Toomre (1964)** [20] devised a factor Q to determine the gravitational stability of a differentially rotating disk of stars. This factor is essential to consider in spiral galaxy evolution.

1.2.2 Resonances in spiral galaxies

The general orbits of stars in a galaxy are not closed; instead, they form rosette patterns. This is because the angular (or azimuthal) frequencies Ω and epicyclic (or radial) frequencies κ fo stars are not always in integral ratios. However, in the non-inertial frame rotating with pattern speed Ω_p, star completing n orbits and m epicyclic oscillations will have closed orbits. These orbits satisfy the relation -

$$\Omega_p = \Omega - \frac{n}{m}\kappa \tag{1.1}$$

Resonances occur where the forces on an orbiting star due to the spiral wave are constant i.e., where their period is the same as the natural period with which a star oscillates about a circular orbit. Some significant resonances observed in spiral galaxies due to differential rotation are [2] -

- **Corotation resonance (CR):** It occurs at the radius where $\Omega_p = \Omega$. Thus, stars at the corotation radius revolve at Ω_p.

[4]Angular frequency of a non-axisymmetric structure like spiral arms or bar

- **Inner Lindblad resonance (ILR):** It occurs at the radius where $\Omega_p = \Omega - \frac{n}{m}\kappa$. There can be zero, one or two ILRs.

- **Outer Lindblad resonance (OLR):** It occurs at the radius where $\Omega_p = \Omega + \frac{n}{m}\kappa$. There can be one OLR.

Resonances result in amplified epicyclic oscillations, and hence, more collisions. This helps in energy dissipation and angular momentum transfer.

1.2.3 Central bars

It has been observed that two-thirds of all spiral galaxies host a bar in the center. Bars are rigid, triaxial systems and are thought to be regions with many overlapping stellar orbits, with major axes aligned. Bar isophotes can vary from elliptical to boxy or peanut-shaped. Unlike the rest of the galaxy, bars are thought to have definite pattern speeds since they are rigid. In this thesis, it is shown that long peanut-shaped bars can have multiple pattern speeds. Bars correspond to the $(n, m) = (1, 2)$ mode from Equation 1.1. The strength of a bar is determined by a factor [2] -

$$\mathcal{R} = \frac{R_{CR}}{a_b} \tag{1.2}$$

Here, R_{CR} is the corotation radius and a_b is the semi-major axis of the bar. Weak bars have $\mathcal{R} > 1$ i.e., they lie within corotation. Bars with $\mathcal{R} \approx 1$ are said to be *fast* and those with $\mathcal{R} \gg 1$ are *slow*.

1.2.4 Overview of spiral galaxy components

Figure 1.2 shows the various components of spiral galaxies. The following structures are present in most spirals and barred spirals -

- **Spiral arms:** The spiral arms are regions of stars that extend from the center of spiral galaxies in a spiral pattern. They are prominent because they contain many bright, young, blue stars.

- **Bulge:** The bulge is a tightly packed, centrally located stellar system that is thicker than the disk, and mostly consists of old, red stars with low metallicities[5].

- **Bar:** The bar is an elongated, smooth stellar system at the center of the galactic disk. It can be thought of as a triaxial bulge.

[5]The ahbundance of elements present in an object that are heavier than hydrogen or helium

- **Thin disk:** The thin disk contributes to most of the stars, mostly young with high metallicities, in the Galactic plane.
- **Thick disk:** The thick disk is thicker and less dense than the thin disk, and is composed almost exclusively of older stars.
- **Galactic halo:** The galactic halo is an extended, roughly spherical component of a galaxy. The *stellar halo* contains old stars of low metallicity, and the *dark halo* is thought to contain dark matter.

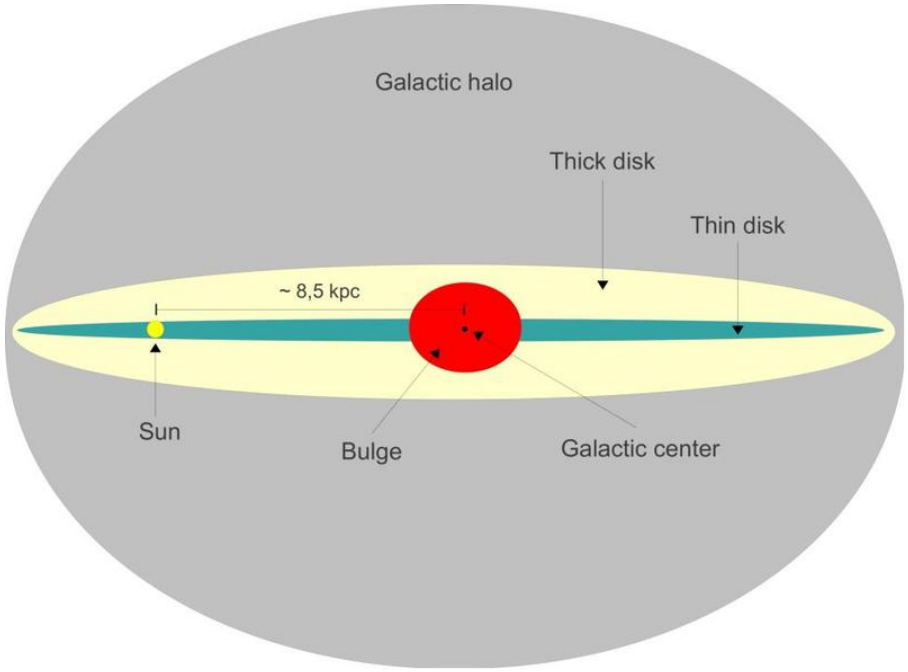

Figure 1.2: Schematic edge-on view of the Milky Way galaxy (Gaba p)

1.3 Multiple pattern speeds in galaxies

The Lin-Shu and other earlier hypotheses assumed that the pattern speeds of spiral arms and bars are the same. Another earlier assumption was that the bar ends at the corotation radius and that the spiral arms lie outside the corotation region. However, studies show that this assumption is false. **Sellwood & Sparke (1988)** [17] show that spiral arms have lower pattern speeds, but still coexist with the bar. Simulations show that the spiral arms can *detach* from and *reattach* to the bar, and can lie partly within the corotation radius. **Sellwood (1993)** [18] argues that even though bars (and rings, which are due to bar resonances) are long-lived features of galaxies, spiral arms can be short-lived resonances.

Since spiral arms and bars are radial features, it can be assumed that the pattern speed at a specific radius is constant. Moreover, there can be a radial dependence of pattern speed. **Meidt et al. (2008a)** [11] and **Meidt et al. (2008b)** [12] have developed and tested a generalized version of the TW method (discussed later) - the radial TW (or TWR) method. However, this procedure is much more complex and is out of the scope of this thesis.

1.4 Evolution of pattern speed with time

Numerical simulations show that bar pattern speeds decrease with time. This cannot be inferred from real data, since we observe single snapshots. In this thesis, multiple time snapshots simulated galaxies are analyzed, and the time-evolution of pattern speeds is noted. The main reason for the decrease in pattern speeds is *angular momentum transfer*. Spiral structure produces a spiral gravitational field, which exerts torques and transfers angular momentum from one part of the disk to another. This angular momentum transfer happens at Lindblad and corotation resonances, from the inner disk or bar to the outer disk or halo. **Lynden-Bell & Kalnajs (1972)** [10] theorize that this process of angular momentum transfer generates spiral structure. **Weinberg (1985)** [22] uses n-body simulations to show how dynamical friction[6] (or Chandrashekha friction) helps in the slowdown of the bar and, subsequently, angular momentum transfer from bar to halo. The assumptions are that the halo is an isothermal sphere, that the bar rotates rigidly and that the torque on the bar is from bar-halo interaction.

[6]Loss of momentum and kinetic energy of moving bodies through gravitational interactions with surrounding matter in space (gravitational drag)

2 Methods

Many methods have been used to measure the pattern speed of the Milky Way Galaxy. These mostly involve finding the rotation curve and Lindblad resonances of the Galaxy to deduce Ω_p. **Lin & Shu (1967)** [9] deduced the value of by assuming the location of the ILR of the Milky Way. **Yuan (1969a)** [23] used the neutral hydrogen profile of the Milky Way to get a value of $13.5\,\mathrm{km\ s^{-1}\ kpc^{-1}}$, with agreeable values, and **Yuan (1969b)** [24] updated this by considering the migration of stars. However, such methods cannot be used for other galaxies since it is not easy to deduce resonances and rotation curves. One such method, independent of model parameters, is described below and used extensively in this thesis.

2.1 The TW method

The method devised by **Tremaine & Weinberg (1984)** [21] is a *model-independent* procedure to calculate pattern speed of a barred galaxy using only astronomical observables - *surface brightness distribution* of a tracer[1] and *radial velocity profile*.

2.1.1 Assumptions and description

There are three key assumptions made.

1. *The galactic disk is flat*

   Let (X, Y) be the coordinates in the galactic plane and (x, y) be the coordinates in the sky plane (as viewed by us). Here, the X-axis is considered to be the *line of nodes*[2] (or the major axis). If the angle of inclination of the galaxy is i, then -

   $$(X, Y) = (x, y\cos i) \tag{2.1}$$

2. *There is a well defined rigid pattern speed*

   Let Ω_p be the pattern speed of the rigid spiral structure, and $\Sigma(x, y, t)$ be the surface brightness distribution. Thus, in the frame of rotation of the galaxy $(r, \phi - \Omega_p t)$, Σ should remain constant =

   $$\Sigma(x, y, t) = \overline{\Sigma}(r, \phi - \Omega_p t) \tag{2.2}$$

[1] Any structure or component of the galaxy which has a global spread

[2] The line on the galactic plane which is not rotated due to inclination

3. *The surface brightness tracer follows the continuity equation*

If $\Sigma(x, y, t)$ follows the continuity equation, we can write -

$$\frac{\partial \Sigma(x,y,t)}{\partial t} + \frac{\partial}{\partial x}\left[\Sigma(x,y,t) v_x(x,y,t)\right] + \frac{\partial}{\partial y}\left[\Sigma(x,y,t) v_y(x,y,t)\right] = 0 \tag{2.3}$$

From Equations 2.2 and 2.3, one can write -

$$\frac{\partial \Sigma(x,y,t)}{\partial t} = -\Omega_p \frac{\partial \overline{\Sigma}(r,\phi)}{\partial \phi} = \Omega_p \left(y \frac{\partial \Sigma}{\partial x} - x \frac{\partial \Sigma}{\partial y} \right) \tag{2.4}$$

Integrating Equation 2.4 first w.r.t. x and then w.r.t. y from $-\infty$ to ∞, and subsequently using Equation 2.1, one can write -

$$\Omega_p \sin i = \frac{\displaystyle\int_{-\infty}^{\infty} \Sigma(X,Y) V_{||}(X,Y)\, \mathrm{d}X}{\displaystyle\int_{-\infty}^{\infty} \Sigma(X,Y) X\, \mathrm{d}X} \tag{2.5}$$

The above equation is an excellent estimate for $\Omega_p \sin i$. Typically, one integrates the numerator and denominator along multiple slits parallel to the line of nodes, and plots the quantities. The slope of the resulting plot gives $\Omega_p \sin i$.

However, **Merrifeld & Kuijken (1995)** [13] found that this result can be improved by using *surface brightness normalized* quantities instead. Thus, Equation 2.5 changes to -

$$\Omega_p \sin i = \left(\frac{\displaystyle\int_{-\infty}^{\infty} \Sigma(X,Y) V_{||}(X,Y)\, \mathrm{d}X}{\displaystyle\int_{-\infty}^{\infty} \Sigma(X,Y)\, \mathrm{d}X} \right) \left(\frac{\displaystyle\int_{-\infty}^{\infty} \Sigma(X,Y)\, \mathrm{d}X}{\displaystyle\int_{-\infty}^{\infty} \Sigma(X,Y) X\, \mathrm{d}X} \right) = \frac{\langle V_{||} \rangle}{\langle X \rangle} \tag{2.6}$$

$$\langle x \rangle = \frac{\displaystyle\sum_{x=-L}^{L} \Sigma(x, st) x\, \mathrm{d}x}{\displaystyle\sum_{-L}^{L} \Sigma(x, st)\, \mathrm{d}x} \tag{2.7}$$

$$\langle v_{los} \rangle = \frac{\displaystyle\sum_{x=-L}^{L} \Sigma(x, st) v(x, st)\, \mathrm{d}x}{\displaystyle\sum_{-L}^{L} \Sigma(x, st)\, \mathrm{d}x} \tag{2.8}$$

2.1.2 Nuances of the TW method

When the TW method was first devised, *long-slit spectroscopy* (LSS) was the norm for extracting spatially resolved spectra. LSS is ideal for the TW method since the method needs

1D line surface brightness and redial velocity profiles. Nevertheless, the advent of *integral field spectroscopy* (IFS) - with 2D resolved spectra - has benefited the application of the TW method.

A crucial requirement of this method is that the surface brightness tracer should follow the continuity equation. The obvious tracer to use is stellar light, which is suitable for early-type galaxies with little dust and negligible star formation. Using LLS and stellar light as a tracer, **Merrifeld & Kuijken (1995)** [13] and **Gerssen, Kuijken & Merrifield (1999)** [6] made the earliest bar pattern speed calculations of NGC 936 and NGC 4596, respectively. However, one must be cautious in choosing a tracer for galaxies with active star-forming regions. With time, other tracers have been found to follow continuity suitably. **Zimmer, Rand & McGraw (2004)** [25],**Rand & Wallin (2004)** [14] use CO as a tracer, and **Hernandez et al. (2005)** [7], **Emsellem et al. (2006)** [4] use Hα instead. The results from using CO and Hα agree. **Aguerri et al. (2015)** [1] and **Garma-Oehmichen et al. (2020)** [5] use IFS images from CALIFA and MaNGA SDSS-IV to calculate bar pattern speeds.

The TW method dictates that the slits chosen must be parallel to the line of nodes, which corresponds to the major axis of the projected galaxy. The angle of inclination can be inferred from the eccentricity ϵ of the elliptical projection. The method also requires the galaxy to be inclined at an angle middling 0° (face-on) and 90° (edge-on), without being close to either. The reasoning is simple. Low inclination galaxies have a negligible radial velocity profile, with huge errors in stellar velocity. High inclination galaxies have bad surface brightness resolution, with surface features overlapped. After judging that a snapshot is suitable for the application of the TW method, slits can be placed. One has to note that there are errors involved in choosing the length and alignment (position angle) of slits, and their proper centering. These errors are discussed by **Garma-Oehmichen et al. (2020)** [5]. On average, the position uncertainties range $\sim 15\%$, the slit length $\sim 9\%$, and the centring error $\sim 5\%$.

2.2 The code

The programming language used is Python. Essential Python packages include -

- `numpy` for manipulating 1D and 2D arrays.
- `matplotlib` for seamless plotting.
- `astropy` for handling *.fits* files.

- `scipy` for scientific operations/tasks.

In this thesis, pattern speeds of *simulated* galaxies are estimated. Detailed information about the simulations is given in Chapters 3 and 4. The relevant Python code is available on github.

gnuplot is used for detailed linear and non-linear fitting. For such tasks, gnuplot performs better than `matplotlib`.

2.2.1 Image analysis

Each snapshot of a simulation consists of two *.fits* images - 2D surface density and line-of-sight (LOS) velocity profiles. Before 1D line profile extraction, these images must be analyzed. One needs to identify the region where the bar dominates, and handle it separately from the spiral arm region. This is necessary for placing slits and subsequent line profile extraction. Chapters 3 and 4 go into more detail about how slits are chosen.

2.2.2 Line profile extraction and interpolation

Once the required slits are placed on the surface density and LOS velocity images, the slit line profiles can be extracted into a `numpy` array. Spline interpolation is performed on the extracted data to improve resolution.

2.2.3 Integration and fitting

The interpolated profiles are integrated (Simpson's rule) to calculate the quantities $\int_{-\infty}^{\infty} \Sigma(X,Y) V_{||}(X,Y)\,\mathrm{d}X$ and $\int_{-\infty}^{\infty} \Sigma(X,Y) X\,\mathrm{d}X$ for every slit. These two quantities, normalized by $\int_{-\infty}^{\infty} \Sigma(X,Y)\,\mathrm{d}X$, are plotted. The slope of the resulting graph is the quantity $\Omega_p \sin i$, as discussed before.

2.2.4 Time evolution of pattern speeds

Pattern speeds are calculated for each snapshot of a simulation. Thus, time evolution of pattern speeds can be deduced. Chapters 3 and 4 show that pattern speeds invariable decrease with time. However, the manner of decrease varies from galaxy to galaxy.

3 Simulation of a barred spiral galaxy

3.1 Description

The first simulation set is the one used by **Saha, Martinez-Valpuesta & Gerhard (2012)** [15]. The GADGET code by **Springel, Yoshida & White (2001)** [19] is used for this purpose. The simulation details are given in Table 3.1.

Property	**Value**
Disk scale length	$R_d = 4.0\,\mathrm{kpc}$
Disk scale height	$h_d = 42\,\mathrm{pc}$
Disk mass	$M_d = 4.5 \times 10^{10}\,\mathrm{M}_\odot$
Bulge mass	$M_b = 3.0 \times 10^{9}\,\mathrm{M}_\odot$
Halo mass	$M_h = 1.82 \times 10^{11}\,\mathrm{M}_\odot$
Toomre Q	$Q = 1.4$
Integration time step	$t = 0.4\,\mathrm{Myr}$
Time between snapshots	$dT = 37.5\,\mathrm{Myr}$
Total evolution time	$T = 2.1\,\mathrm{Gyr}$
Number of particles	$N = 1.0 \times 10^{7}$
Disk particle mass	$m_d = 1.2 \times 10^{4}\,\mathrm{M}_\odot$
Bulge particle mass	$m_b = 0.3 \times 10^{4}\,\mathrm{M}_\odot$
Halo particle mass	$m_h = 3.6 \times 10^{4}\,\mathrm{M}_\odot$

Table 3.1: Simulation 1 parameters

At the start of the simulation, surface density of the simulated galaxy is axisymmetric with an exponential radial profile and a $\mathrm{sech}^2 z$ vertical profile.
In total, 57 snapshots of the simulation are extracted, with the time difference between consecutive snapshots being -

$$dT = 37.5\,\mathrm{Myr} \tag{3.1}$$

Figure 3.1 shows every 8th snapshot at an inclination angle $i = 30°$. The width of each image is $2 \times 10R_d = 80.0\,\mathrm{kpc}$. Since each image has the dimension $256\,\mathrm{px} \times 256\,\mathrm{px}$, one can convert

pixel values to kpc -

$$1\,\mathrm{px} = \frac{5}{16}\,\mathrm{kpc} = 0.3125\,\mathrm{kpc} \tag{3.2}$$

Thus, pattern speed units for the simulation can be converted as follows -

$$1\,\mathrm{km\ s^{-1}\ px^{-1}} = \frac{16}{5}\,\mathrm{km\ s^{-1}\ kpc^{-1}} = 3.2\,\mathrm{km\ s^{-1}\ kpc^{-1}} \tag{3.3}$$

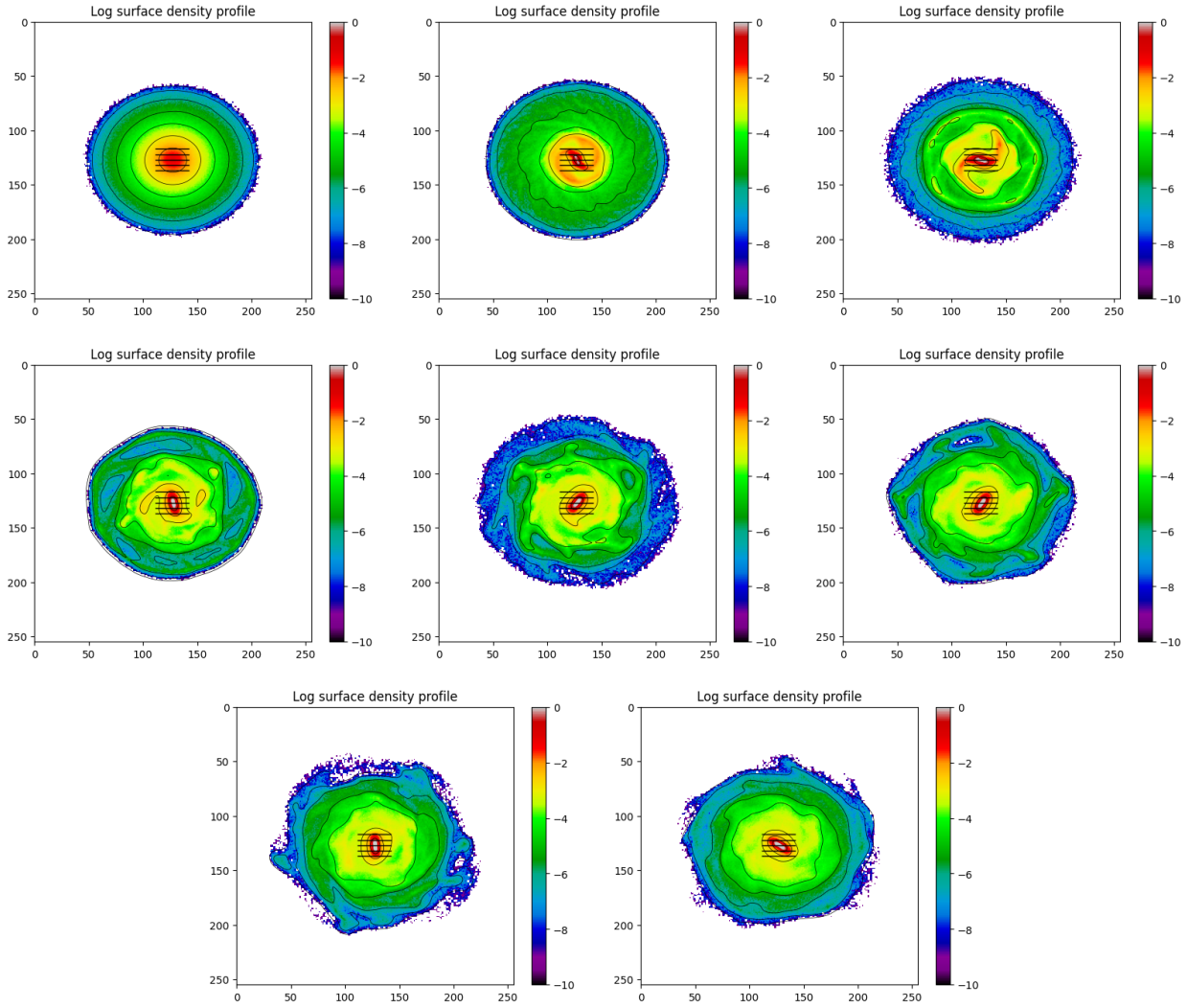

Figure 3.1: Log surface density of every 8th snapshot (300 Myr gap) with $i = 30°$ and $1\,\mathrm{px} = 0.3125\,\mathrm{kpc}$

Figure 3.1 shows the various stages of the simulation. Starting from a completely axisymmetric surface density distribution, the first hint of a weak bar is seen at snapshot 008 (~ 300 Myr). At this point, the region around the bar is still in the process of spiraling out, but no clear spiral arms have formed. By snapshot 016 (~ 600 Myr), this neighborhood has cleared out, and clear arms can be observed. As time passes, one can observe that the spiral arms strengthen and weaken, but never become very prominent. For example, at snapshots 024 (~ 900 Myr),

031 ($\sim$ 1.16 Gyr) and 038 ($\sim$ 1.16 Gyr), the arms weaken. After snapshot 308, the strength does not pick up again, and this continues till the end, up to snapshot 056 ($\sim$ 2.1 Gyr).

3.2 Results

3.2.1 Pattern speed of the central bar

Figure 3.2 depicts the log surface density and LOS velocity profiles of snapshot 035 of the simulation. The slits are restricted to the central region to avoid contribution from the rest of the galaxy. The half-slit width is chosen to be $L = 15$ px. Beyond this region, it can be assumed that the bar does not exist i.e., the bar surface density goes to zero.

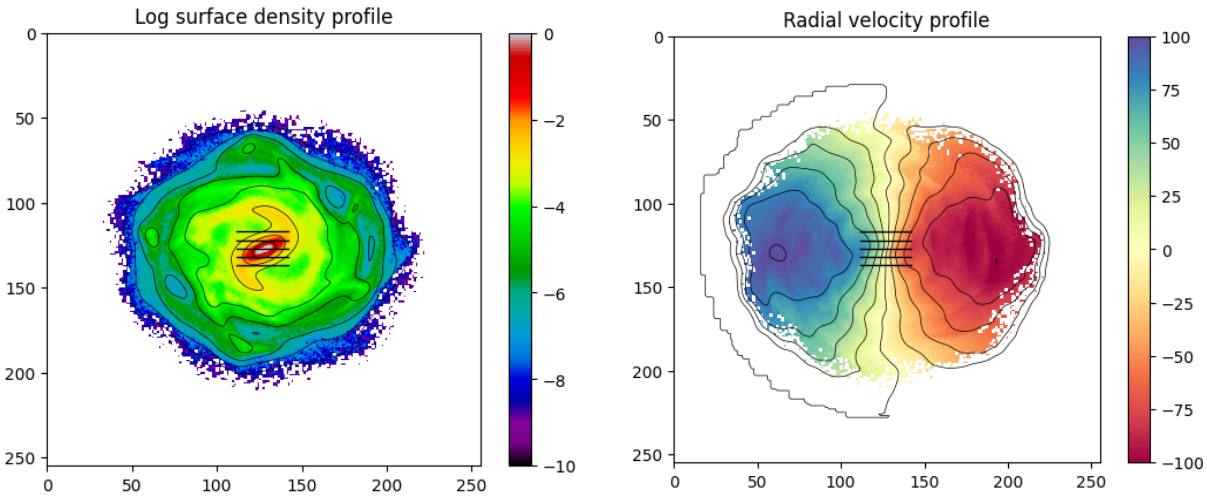

Figure 3.2: Log surface density and LOS velocity profiles of snapshot 035, with slits along the central bar ($i = 30°$ and 1 px = 0.3125 kpc)

The snapshot 035 has been chosen for an example because it is ideal for applying the TW method. This snapshot has the central bar at an intermediate angle between the major and the minor axes, due to which the quantities $\langle x \rangle$ and $\langle v_{los} \rangle$ are not close to 0. This problem arises in snapshots where the bar is very close to either the vertical or the horizontal.

After finding the center of the surface density of the galaxy, line profiles are extracted at different slits parallel to the line of nodes. After interpolation, the profiles can be integrated to calculate the quantities in Equation 2.6.

The quantities $\langle x \rangle$ and $\langle v_{los} \rangle$ are measured for different slit translations st with half-slit width $L = 15\,\text{px}$. The subsequent plots are shown in Figure 3.3. The slopes of both should ideally equal $\Omega_p \sin i$, but it is seen that the second plot is a much better fit. This is further emphasized by the fit parameters of the two plots -

- *(Usual)* Slope $m = -4.80 \pm 0.25$, Sum of squares of residuals = 2092.86
- *(Normalized)* Slope $m = -4.73 \pm 0.05$, Sum of squares of residuals = 1.78

The normalized fit is indeed better. Henceforth, all pattern speed measurements will be done using the normalized quantities $\langle x \rangle$ and $\langle v_{los} \rangle$.

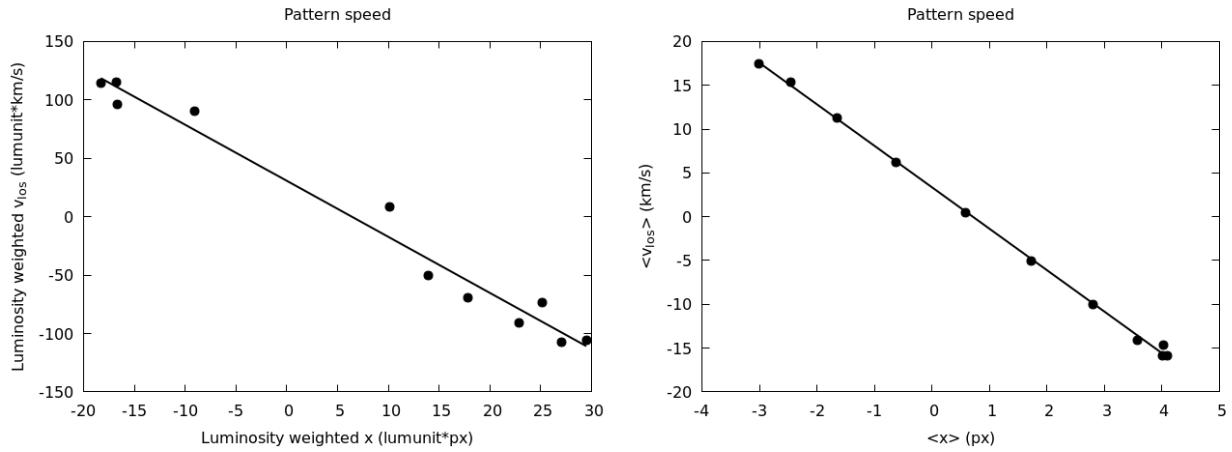

Figure 3.3: Better fit for pattern speed is obtained by plotting luminosity normalized $\langle x \rangle$ and $\langle v_{los} \rangle$ (half-slit width $L = 15\,\text{px}$)

To verify that the goodness of the value of L, the variation of calculated pattern speed with respect to the half-slit width L is noted. Figure 3.4 shows this plot. It is observed that for half-slit widths up to 15 px, the calculated bar pattern speed remains more or less constant at $\sim$ 4.5–5 km s^{-1} px^{-1}. At higher half-slit widths, the values of bar pattern speed decrease. This is due to the effect of the spiral arms - they rotate slower than the bar and thus, reduce the values. It is also observed that the error in pattern speed increases with half-slit width, presumably due to the same reason.

For each of the 57 snapshots, the bar pattern speeds are calculated. Using the conversion factors from Equations 3.1 and 3.3, the pattern speed units can be converted to km s^{-1} kpc^{-1}, and snapshot numbers can be converted to real-time. Figure 3.5 shows the time evolution

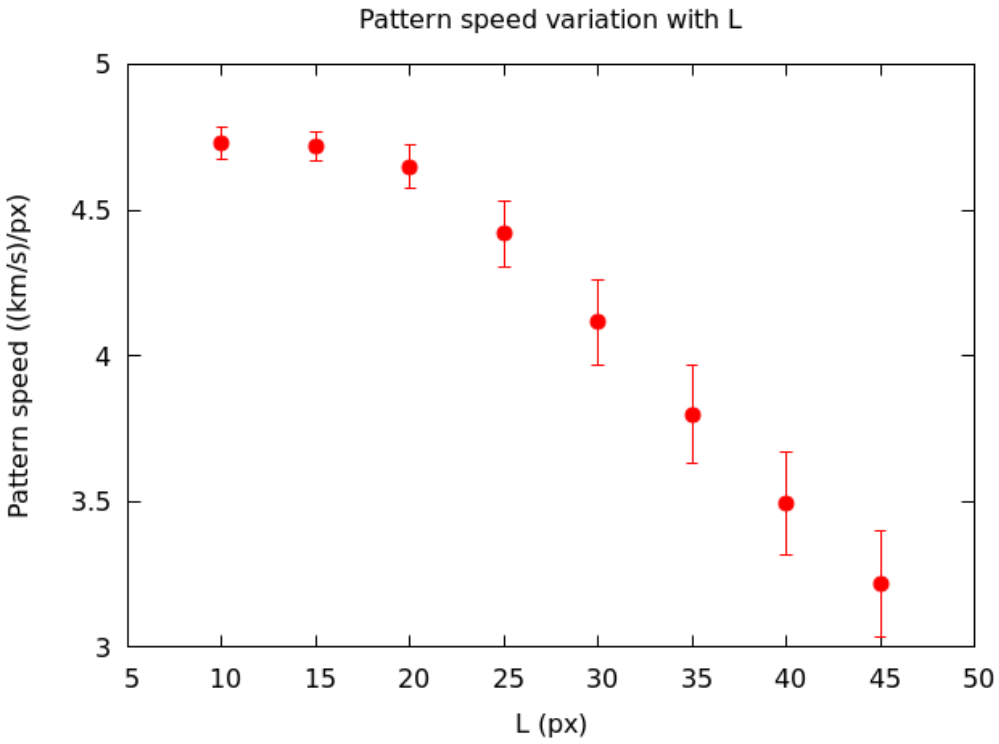

Figure 3.4: Variation of bar pattern speed with half-slit width L

of pattern speeds of the bar. As mentioned before, not all snapshots result in reliable values of pattern speeds (for instance, vertical or horizontal orientations). Thus, pattern speeds with errors beyond a threshold are omitted from the plots. The decrease in pattern speeds seems to be approximately linear. The fit of the form $\Omega_p = \alpha t + \Omega_0$ has best-fit parameters $\alpha = -6.22 \pm 0.57\,\mathrm{km\ s^{-1}\ kpc^{-1}\ Gyr^{-1}}$ (rate of decrease of pattern speed) and $\Omega_0 = 39.00 \pm 0.85\,\mathrm{km\ s^{-1}\ kpc^{-1}}$ (initial pattern speed).

Figure 3.6 shows the histogram of pattern speeds of the bar, along with the mean value of $32.56\,\mathrm{km\ s^{-1}\ kpc^{-1}}$.

3.2.2 Pattern speed of spiral arms using a masked central bar

Now that the pattern speeds of the central bar have been calculated, one needs a method to do the same for the spiral arms. One way to get around the problem of bar contribution is to mask the bar completely. Figure 3.7 depicts the log surface density and LOS velocity profiles of snapshot 035 of the simulation, with the bar region masked. The radius of the bar region is taken to be 15 px. The slits are restricted to the central region, and the half-slit width is chosen to be $L = 50$ px. Beyond this region, the spiral arm density is negligible. Since the central bar is masked, the only expected contribution to the pattern speed calculation is of the spiral arms.

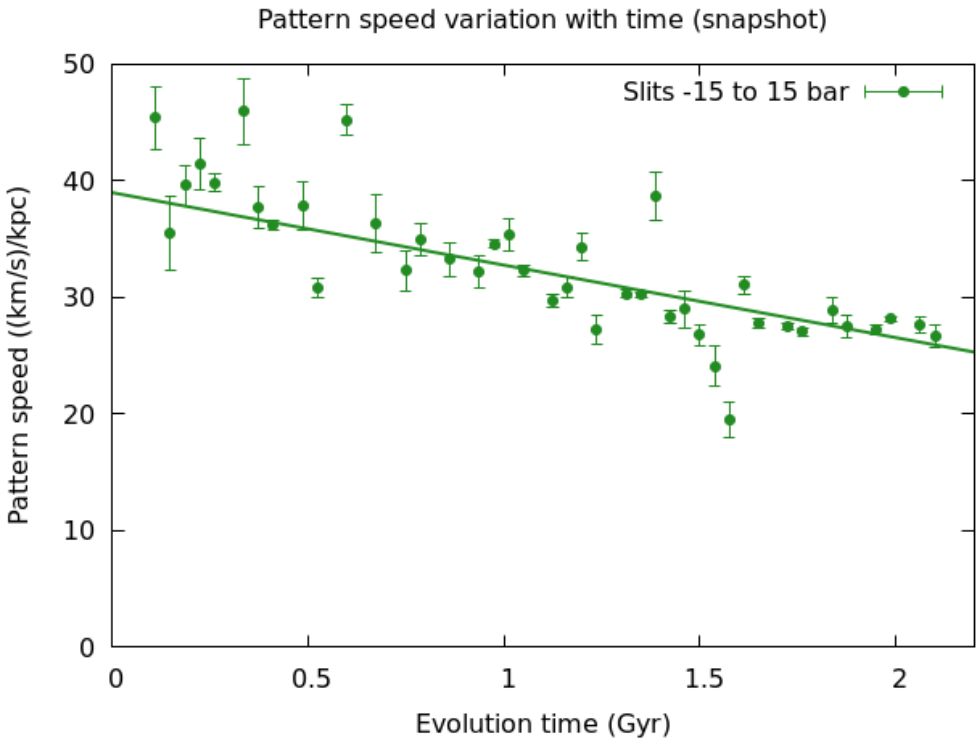

Figure 3.5: Decrease of pattern speed of the central bar with time, fit linearly

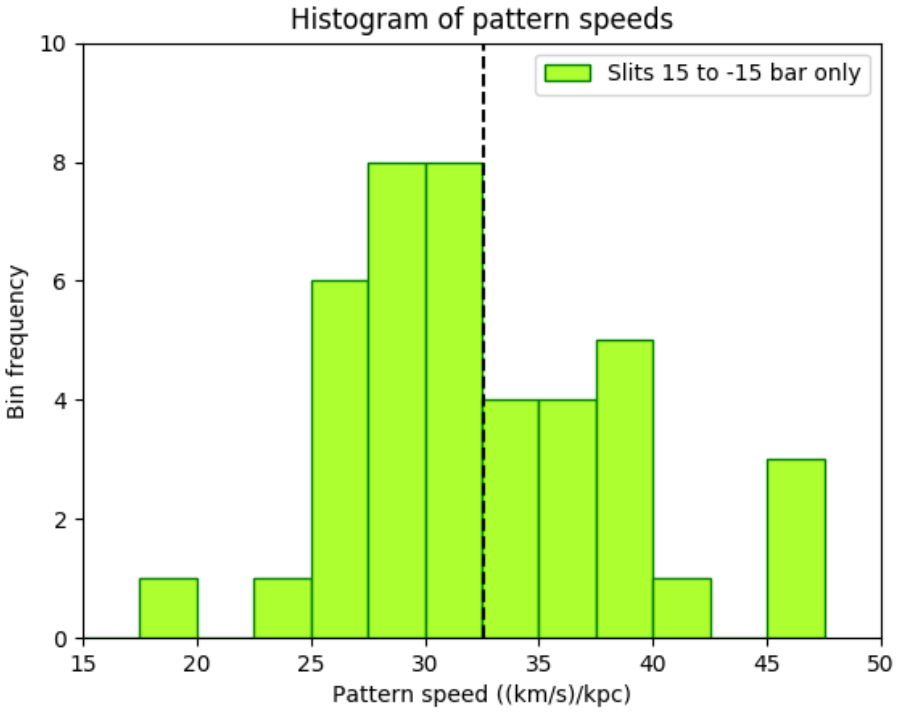

Figure 3.6: Histogram of pattern speeds of the central bar

As before, spiral arm pattern speeds (with masked bar) are calculated for all 57 snapshots,

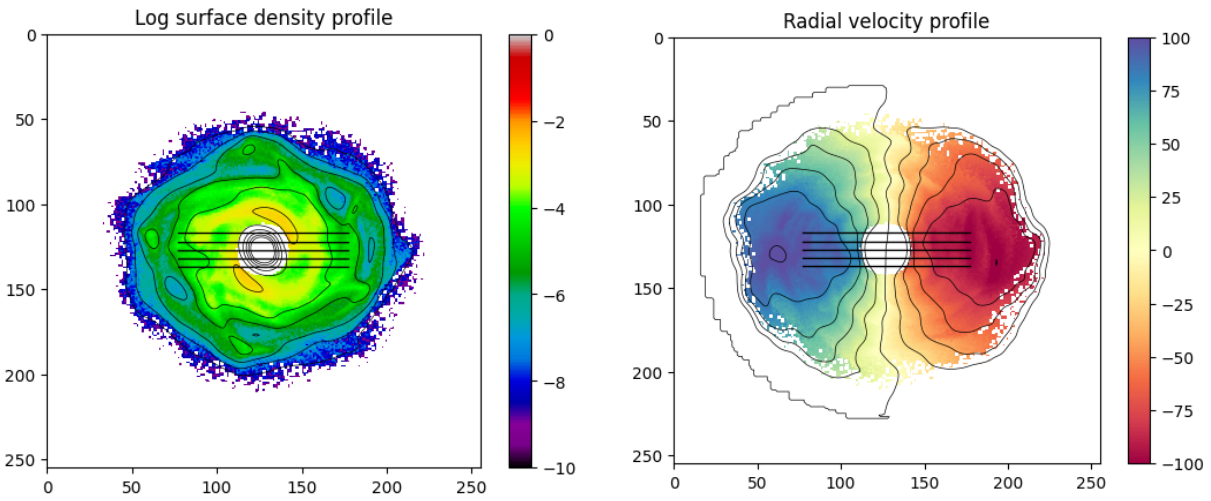

Figure 3.7: Log surface density and LOS velocity profiles of snapshot 035, with central slits and a masked bar ($i = 30°$ and $1\,\mathrm{px} = 0.3125\,\mathrm{kpc}$)

and the unit conversions are done. Figure 3.8 shows the time evolution of pattern speeds of the spiral arms (with masked bar). The plot shows that the calculated pattern speeds vary quite a bit. Moreover, the number of values with errors less than the threshold is much lesser than before. These two facts lead one to conclude that the method of masking the bar is not a reliable way to calculate spiral arm pattern speeds.

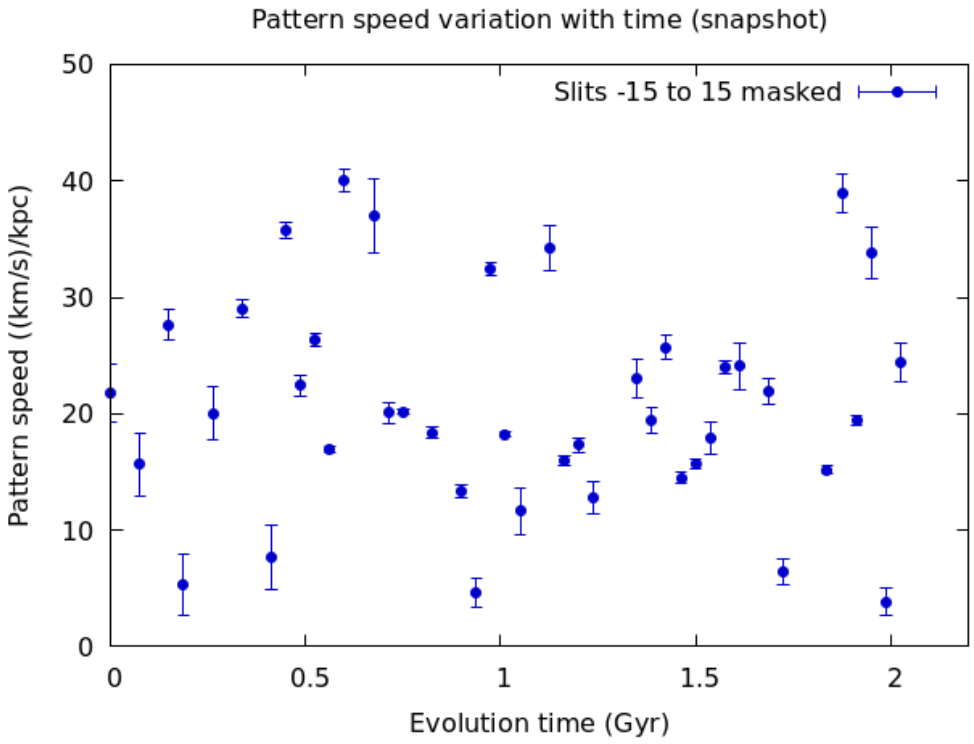

Figure 3.8: Decrease of pattern speed of spiral arms (with masked bar) with time - very scattered

Figure 3.9 shows the histogram of pattern speeds of the spiral arms (with masked bar), along with the mean value of 20.80 km s^{-1} kpc^{-1}. As expected, the spiral arm pattern speeds are lesser than those of the bar. However, the method of calculating spiral arm pattern speeds needs to be modified. In the next subsection, one such method is shown.

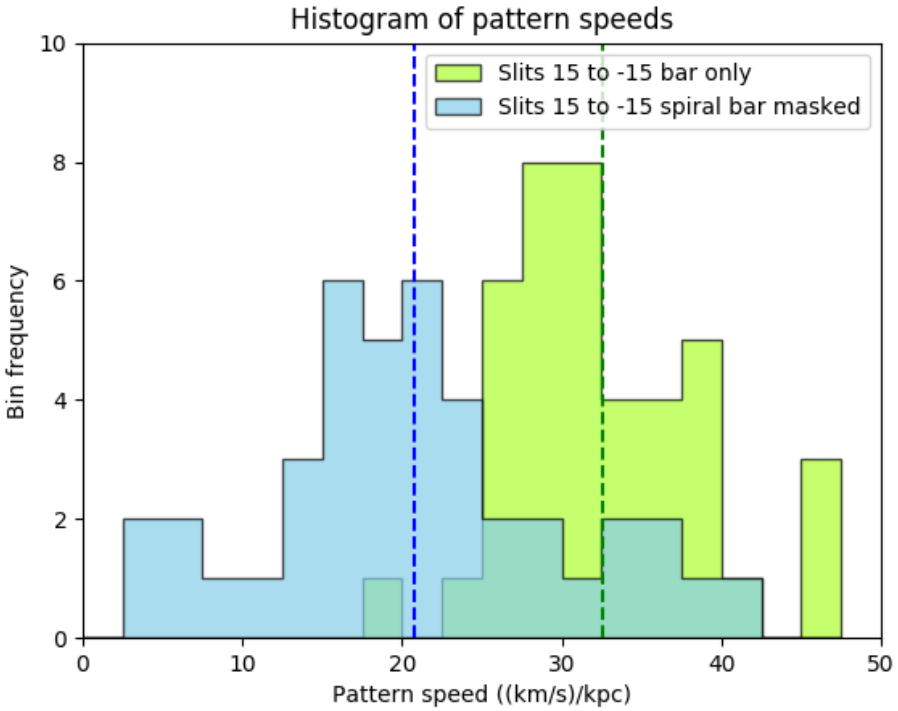

Figure 3.9: Histogram of pattern speeds of the central bar and spiral arms (with masked bar)

3.2.3 Pattern speed of spiral arms using vertically translated slits

The method of masking the bar, however logical, does not seem to calculate spiral arm pattern speeds reliably. Instead of masking values, one can use slits which are vertically translated to measure spiral arm pattern speeds. This method has the same reasoning as the previous one - to avoid bar contribution. If the slits are placed far enough from the central region, the bar is not expected to contribute to the pattern speed. Figure 3.10 depicts the log surface density and LOS velocity profiles of snapshot 035 of the simulation, with the slits vertically translated 15 px up and down. The half-slit width is chosen to be $L = 50$ px as before. Beyond this region, the spiral arm density is negligible.

As before, spiral arm pattern speeds (with slits translated) are calculated for all 57 snapshots, and the unit conversions are done. Figure 3.11 shows the time evolution of pattern

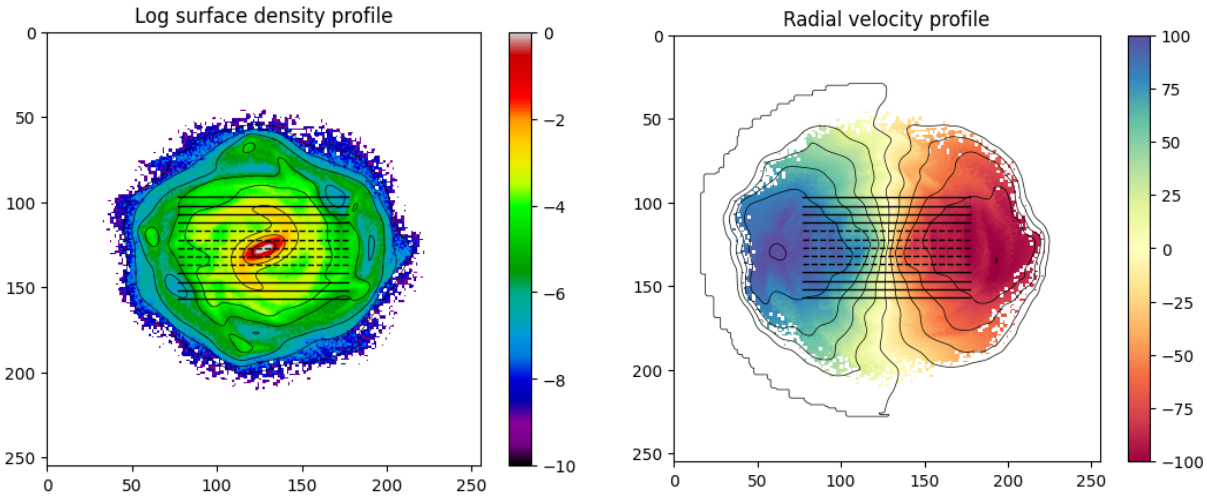

Figure 3.10: Log surface density and LOS velocity profiles of snapshot 035, with slits vertically translated, with slits along the central bar ($i = 30°$ and $1\,\text{px} = 0.3125\,\text{kpc}$)

speeds of the spiral arms (with slits translated). Unlike the masked bar case, this plot shows a clear linear decrease in pattern speeds. Moreover, there are far more values with errors less than the threshold. The conclusion is that the method of slit translation works much better than the one with a masked bar. The fit of the form $\Omega_p = \alpha t + \Omega_0$ has best-fit parameters $\alpha = -3.57 \pm 1.23\,\text{km s}^{-1}\,\text{kpc}^{-1}\,\text{Gyr}^{-1}$ (rate of decrease of pattern speed) and $\Omega_0 = 19.59 \pm 1.65\,\text{km s}^{-1}\,\text{kpc}^{-1}$ (initial pattern speed).

Figure 3.12 shows the histogram of pattern speeds of the spiral arms (with masked bar), along with the mean value of $15.60\,\text{km s}^{-1}\,\text{kpc}^{-1}$. As expected, the spiral arm pattern speeds are lesser than those of the bar.

In the next chapter, another simulated galaxy is analyzed using the slit translation method. The bar masking method is not used since it is erroneous.

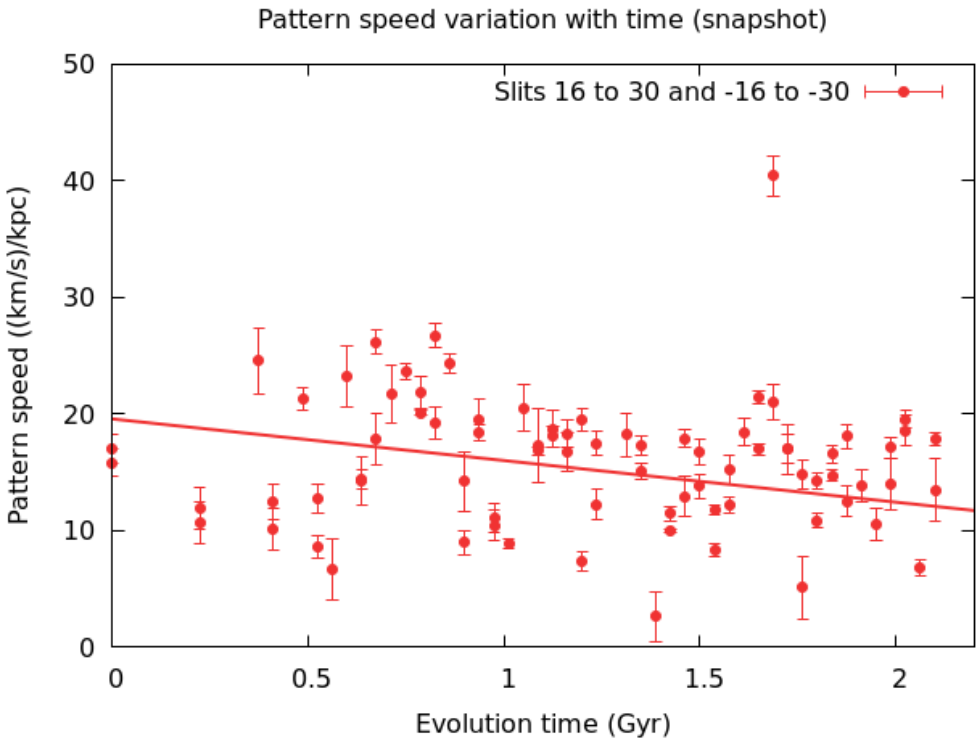

Figure 3.11: Decrease of pattern speed of spiral arms (with slits translated) with time, fit linearly

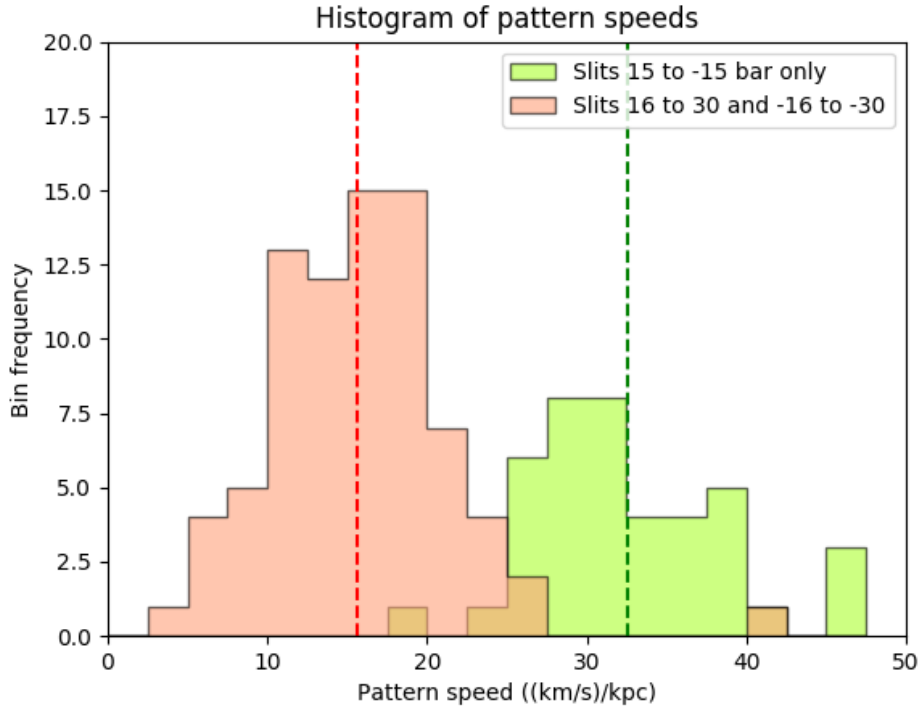

Figure 3.12: Histogram of pattern speeds of the central bar and spiral arms (with slits translated)

4 Simulation of a long-barred galaxy

4.1 Description

The second simulation set is the one used by **Saha, Graham & Rodríguez-Herranz (2018)** [16]. The GADGET code by **Springel, Yoshida & White (2001)** [19] is used for this purpose. The simulation details are given in Table 4.1.

Property	**Value**
Disk scale length	$R_d = 3.0\,\mathrm{kpc}$
Disk mass	$M_d = 1.68 \times 10^{10}\,\mathrm{M}_\odot$
Bulge mass	$M_b = 0.22 \times 10^{9}\,\mathrm{M}_\odot$
Halo mass	$M_h = 6.5 \times 10^{10}\,\mathrm{M}_\odot$
Toomre Q	$Q = 1.15$
Integration time step	$t = 1.9\,\mathrm{Myr}$
Time between snapshots	$dT = 60\,\mathrm{Myr}$
Total evolution time	$T = 13.2\,\mathrm{Gyr}$
Number of particles	$N = 3.7 \times 10^6$
Disk particle mass	$m_d = 1.4 \times 10^4\,\mathrm{M}_\odot$
Bulge particle mass	$m_b = 0.45 \times 10^4\,\mathrm{M}_\odot$
Halo particle mass	$m_h = 3.1 \times 10^4\,\mathrm{M}_\odot$

Table 4.1: Simulation 2 parameters

At the start of the simulation, surface density of the simulated galaxy is axisymmetric with an exponential radial profile and a $\mathrm{sech}^2 z$ vertical profile.

In total, 221 snapshots of the simulation are extracted, with the time difference between consecutive snapshots -

$$dT = 60\,\mathrm{Myr} \tag{4.1}$$

Figure 3.1 shows every 20th snapshot at an inclination angle $i = 30°$. The width of each image is $2 \times 10R_d = 60.0\,\mathrm{kpc}$. Since each image has the dimension $256\,\mathrm{px} \times 256\,\mathrm{px}$, one can convert pixel values to kpc -

$$1\,\mathrm{px} = \frac{15}{64}\,\mathrm{kpc} = 0.234375\,\mathrm{kpc} \tag{4.2}$$

Thus, pattern speed units for the simulation can be converted as follows -

$$1\,\mathrm{km\ s^{-1}\ px^{-1}} = \frac{64}{15}\,\mathrm{km\ s^{-1}\ kpc^{-1}} = 4.2\dot{6}\,\mathrm{km\ s^{-1}\ kpc^{-1}} \tag{4.3}$$

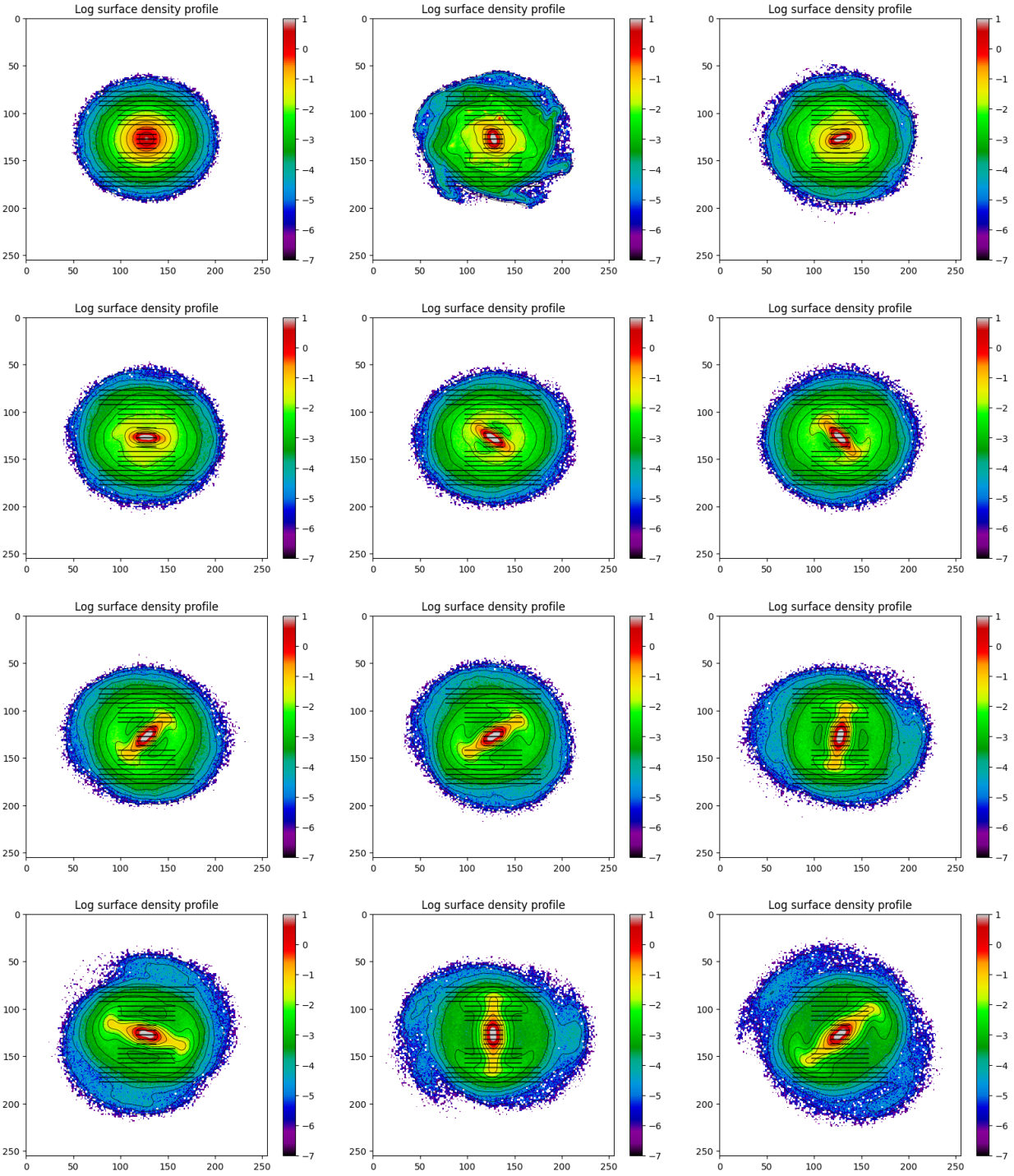

Figure 4.1: Log surface density of every 20th snapshot (1.2 Gyr gap) with $i = 30°$ and $1\,\mathrm{px} = 0.234375\,\mathrm{kpc}$

Figure 4.1 shows the various stages of the simulation. Starting from a completely axisymmetric surface density distribution, the first hint of a weak bar is seen at snapshot 011 ($\sim 650\,\mathrm{Myr}$).

At this point, the region around the bar is very perturbed. By snapshot 035 ($\sim$ 2.1 Gyr), this neighborhood has cleared out, and a small stable bar is observed. As time passes, the bar narrows and lengthens, and becomes stronger. A ring forms around the bar region. The lengthened bar can be seen clearly in snapshot 055 ($\sim$ 3.3 Gyr). The bar profile also becomes *boxy* and eventually, *peanut-shaped*. Snapshot 084 ($\sim$ 5 Gyr) shows the peanut-shaped bar. The bar continues to strengthen and lengthen. The progression of strength can be seen in snapshots 106 ($\sim$ 6.4 Gyr) $\rightarrow$ 135 ($\sim$ 8.1 Gyr) $\rightarrow$ 181 ($\sim$ 10.9 Gyr) $\rightarrow$ 220 ($\sim$ 13.2 Gyr). Ultimately, the bar has a very unique structure - a central boxy profile with two peatnut-shaped lopes at either end. There is no indication of spiral arms in any of the snapshots.

4.2 Results

The log surface density plots in Figure 4.1 depict the placement of slits. As explained for the previous simulation, vertically translated slits are used to determine the pattern speeds of different parts of the galaxy. However, in this simulation, pattern speeds of different parts of the *bar* are calculated (spiral arms are absent). Thus, one can divide an evolved bar into three major regions -

1. **Inner (small central bar):** This region has fairly elliptical contours of surface brightness. The small bar develops fairly early in the simulation. The vertical range is chosen to be -10–10 px with the half-slit length $L = 10$ px.

2. **Outer (peanut-shaped extensions):** This region develops much later, and keeps growing. It is also characterized by a ring of high surface density projecting out from the lobes. The vertical range is chosen to be ± 31– $\pm\, 50$ px with the half-slit length $L = 50$ px.

3. **Intermediate:** This region has a boxy profile of surface brightness. It evolves from a noisy neighborhood around the small central bar, to an intermediate *stem* between the small central bar and the lobes. The vertical range is chosen to be ± 11– $\pm\, 30$ px with the half-slit length $L = 30$ px.

For each of the 221 snapshots, the pattern speeds are calculated for the different bar regions. Using the conversion factors from Equations 4.1 and 4.3, the pattern speed units can be converted to km s^{-1} kpc^{-1}, and snapshot numbers can be converted to real-time. Figures 4.2, 4.3 and 4.4 shows the time evolution of pattern speeds of different regions of the bar. The best-fit parameters are given below -

- **Inner (central small bar):** The fit of the form $\Omega_p = \Omega_0 e^{-\lambda t} + \Omega'$ has best-fit parameters $\lambda = 0.32 \pm 0.04$, $\Omega_0 = 35.15 \pm 4.97\,\mathrm{km\ s^{-1}\ kpc^{-1}}$ and $\Omega' = 0.41 \pm 0.34\,\mathrm{km\ s^{-1}\ kpc^{-1}}$.

- **Outer (peanut-shaped extensions):** The fit of the form $\Omega_p = \alpha t + \Omega_0$ has best-fit parameters $\alpha = -0.38 \pm 0.02\,\mathrm{km\ s^{-1}\ kpc^{-1}\ Gyr^{-1}}$ and $\Omega_0 = 10.83 \pm 0.16\,\mathrm{km\ s^{-1}\ kpc^{-1}}$.

- **Intermediate:** The fit of the form $\Omega_p = \Omega_0 e^{-\lambda t} + \Omega'$ has best-fit parameters $\lambda = 0.24 \pm 0.03$, $\Omega_0 = 17.13 \pm 1.20\,\mathrm{km\ s^{-1}\ kpc^{-1}}$ and $\Omega' = 4.88 \pm 0.52\,\mathrm{km\ s^{-1}\ kpc^{-1}}$.

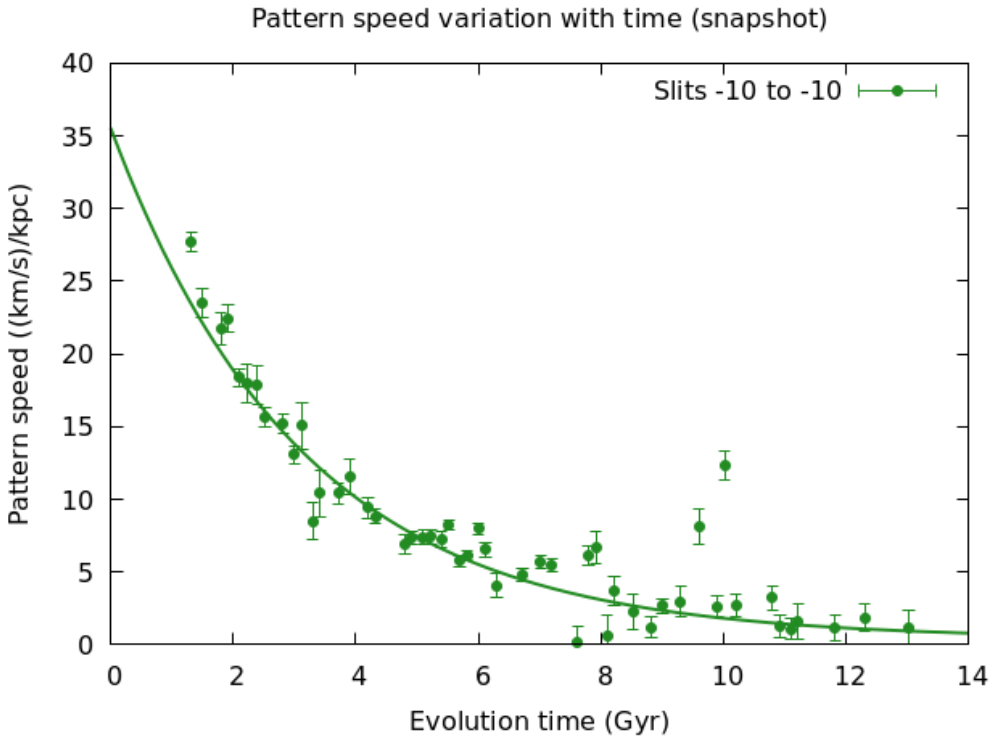

Figure 4.2: Decrease of inner region pattern speed with time, fit exponentially

For better visualization, Figure 4.5 shows the three best-fit curves in the same plot. The graph shows that the decrease in pattern speed of the *inner* region is undoubtedly exponential ($e^{-\lambda t}$) and that of the *outer* region is linear. The *intermediate* region also shows an exponential decrease in pattern speed, but the factor λ is smaller. This is unlike the previous simulation, where the decrease in pattern speeds of both the bar and the spiral arms were linear. The manner decrease in pattern speed is similar to the n-body simulations by **Weinberg (1985)** [22].

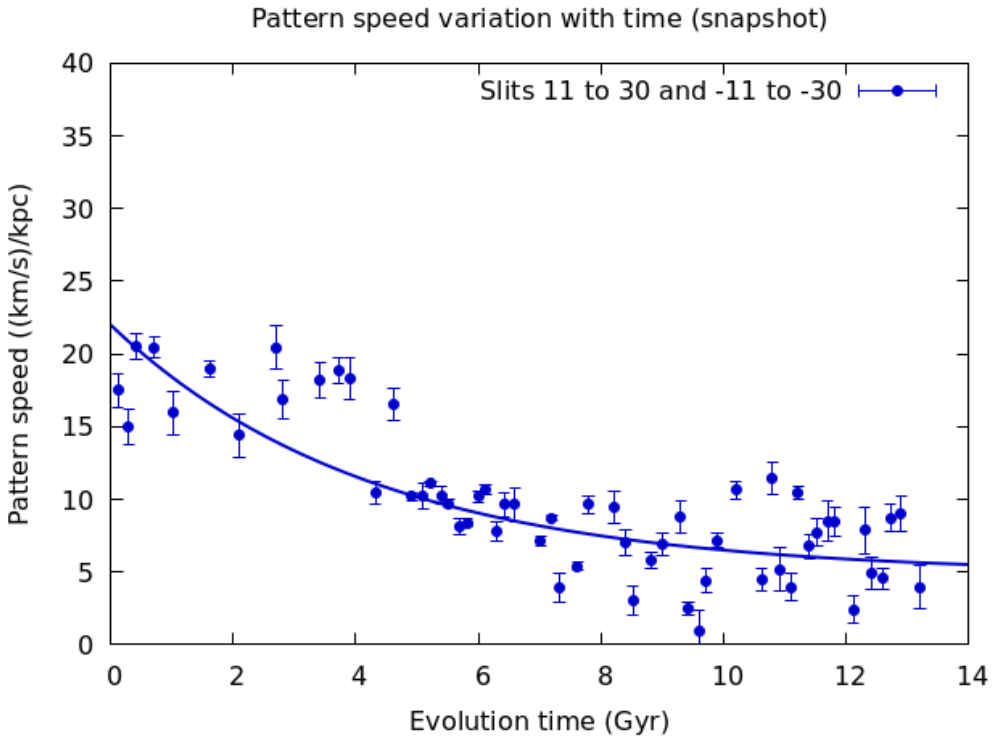

Figure 4.3: Decrease of intermediate region pattern speed with time, fit exponentially

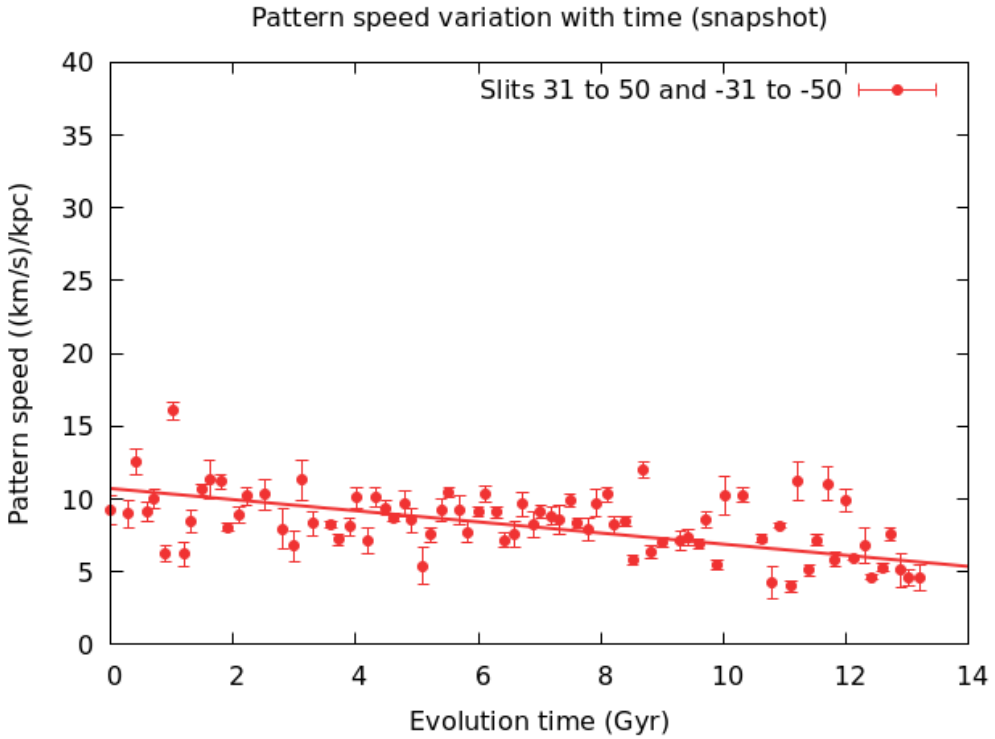

Figure 4.4: Decrease of outer region pattern speed with time, fit linearly

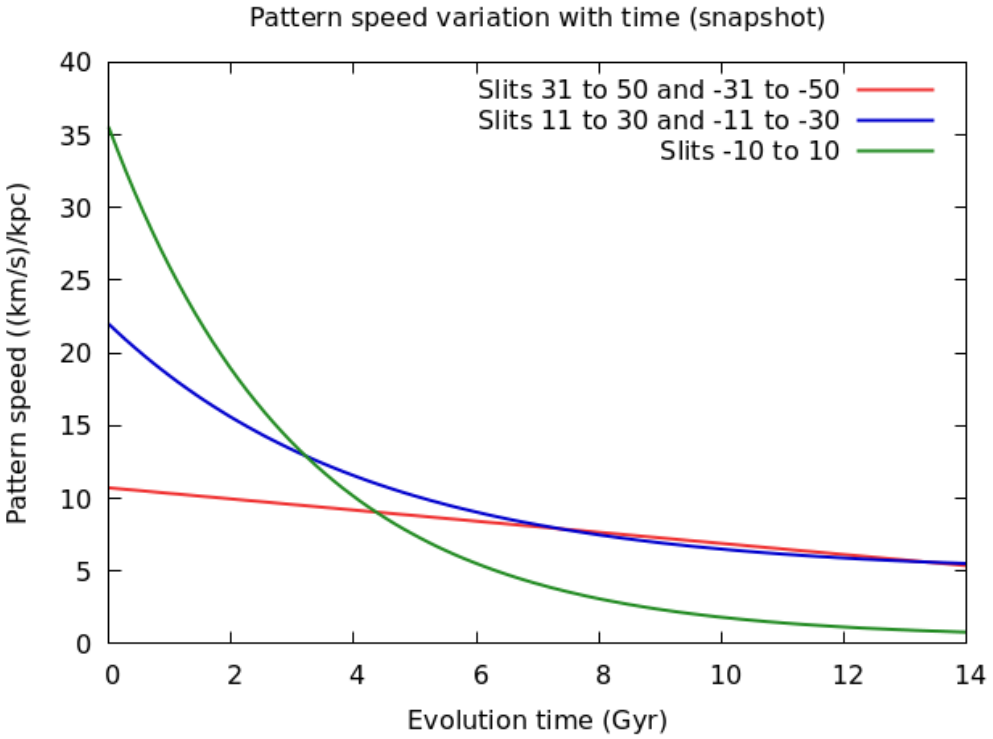

Figure 4.5: Best-fits of decrease of pattern speed with time

5 Conclusion

The TW method is used to calculate pattern speeds of various parts of the galaxy. In *simulation set 1*, the bar and spiral arm pattern speeds are computed. The values of pattern speeds are confirmed using a Fourier method. In this method, the bar position angle at each snapshot is deduced from the phase parameter of the $m = 2$ mode, and angular speeds are hence calculated (time between snapshots is known). Figure 5.1 shows that the TW method is indeed correct. Spiral arm pattern speeds are evaluated using two methods - *masking the bar* and *vertically translating the slits*. Furthermore, it is shown that spiral arm pattern speeds are more precise in the second method, and hence the first method is rejected.

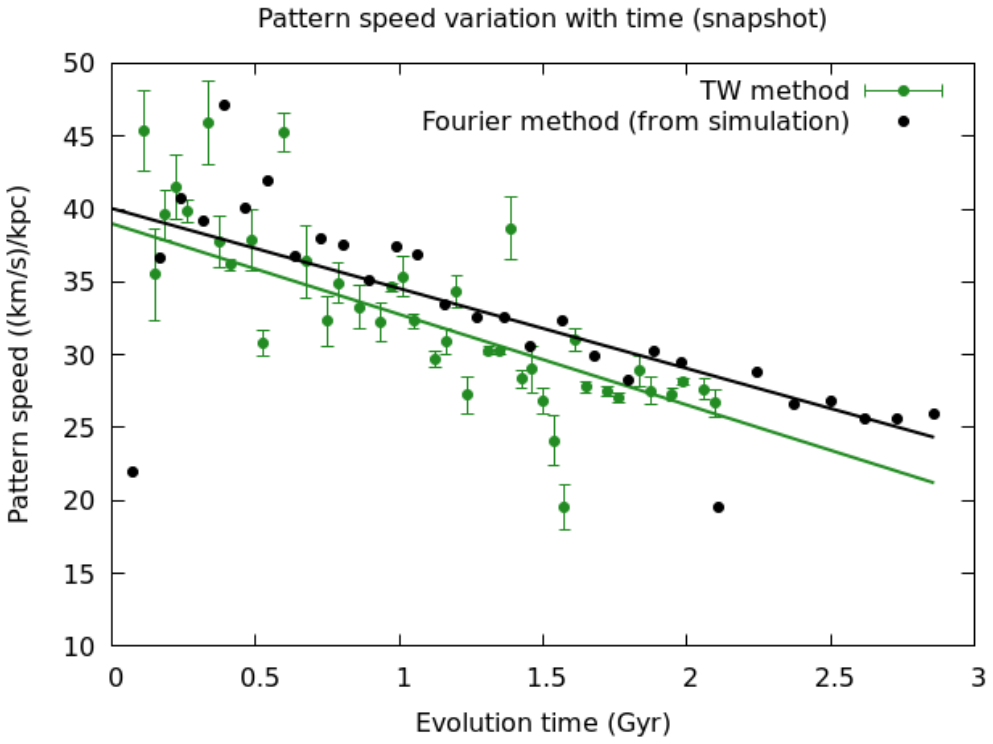

Figure 5.1: Verification of TW method values for bar pattern speed of *simulation set 1*

The bar pattern speeds are clearly higher than those of the spiral arms, which is as expected. The decrease in pattern speeds of both the bar and spiral arms of *simulation set 1* are observed. Both decrease linearly.

In *simulation set 2*, spiral arms are absent. However, the bar grows continuously and shows

peanut-shaped features. The pattern speeds of different *sections* of the bar are evaluated. Surprisingly, it is seen that the manner of decrease of pattern speed of the central part of the bar is exponential. This is different from the the outer part of the bar (the peanut lobes) and the ring, where the decrease is linear. This brings up the question of the mechanism involved in angular momentum transfer. Clearly, there is more than one process involved.

These results need theoretical investigation. One needs to look into the exact method of transfer of angular momentum, and ascertain why the manner of decrease in pattern speeds is linear or exponential.

Bibliography

[1] Aguerri, J. A. L.; Méndez-Abreu, J.; Falcón-Barroso, J.; et al.: *Bar pattern speeds in CALIFA galaxies. I. Fast bars across the Hubble sequence* 2015, A&A, 576, A102

[2] Binney, J.; Tremaine, S.: *Galactic Dynamics* 1987, Princeton University Press

[3] Carroll, B. W.; Ostlie, D. A.: *An Introduction to Modern Astrophysics* 1996, Cambridge University Press

[4] Emsellem, E.; Fathi, K.; Wozniak, H.; Ferruit, P.; Mundell, C. G.; Schinnerer, E.: *Gas and stellar dynamics in NGC 1068: probing the galactic gravitational potential* 2006, MNRAS, 365, 367

[5] Garma-Oehmichen, L.; Cano-Díaz, M.; Hernández-Toledo, H.; Aquino-Ortíz, E.; Valenzuela, O.; Aguerri, J. A. L.; Sánchez, S. F.; Merrifield, M. R.: *SDSS-IV MaNGA: Bar pattern speed estimates with the Tremaine-Weinberg method and their error sources* 2020, MNRAS, 491, 3655

[6] Gerssen, J.; Kuijken, K.; Merrifield, M. R.: *The pattern speed of the bar in NGC 4596* 1999, MNRAS, 306, 926

[7] Hernandez, O.; Wozniak, H.; Carignan, C.; Amram. P.; Chemin, L.; Daigle, O.: *On the Relevance of the Tremaine-Weinberg Method Applied to an Hα Velocity Field: Pattern Speed Determination in M100 (NGC 4321)* 2005, ApJ, 632, 253

[8] Lin, C. C.; Shu, F. H.: *On the Spiral Structure of Disk Galaxies* 1964, ApJ, 140, 646

[9] Lin, C. C.; Shu, F. H.: *Density waves in disk galaxies* 1967, IAU Symp. 31.

[10] Lynden-Bell, D.; Kalnajs, A. J.: *On the generating mechanism of spiral structure* 1972, MNRAS, 157, 1

[11] Meidt, S. E.; Rand, R. J.; Merrifield, M. R.; Debattista, V. P.; Shen, J.: *Tests of the Radial Tremaine-Weinberg Method* 2008, ApJ, 676, 899

[12] Meidt, S. E.; Rand, R. J.; Merrifield, M. R.; Shetty, R.; Vogel, S. N.: *Radial Dependence of the Pattern Speed of M51* 2008, ApJ, 688, 244

[13] Merrifield, M. R.; Kuijken, K.: *The pattern speed of the bar in NGC 936* 1995, MNRAS, 274, 933

[14] Rand, R. J.; Wallin, J. F.: *Pattern Speeds of BIMA SONG Galaxies with Molecule-dominated Interstellar Mediums Using the Tremaine-Weinberg Method* 2004, ApJ, 614, 142

[15] Saha, K.; Martinez-Valpuesta, I.; Gerhard, O.: *Spin-up of low-mass classical bulges in barred galaxies* 2012, MNRAS, 421, 333

[16] Saha, K.; Graham, A. W.; Rodríguez-Herranz, I.: *Building the Peanut: Simulations and Observations of Peanut-shaped Structures and Ansae in Face-on Disk Galaxies* 2018, ApJ, 852, 133

[17] Sellwood, J. A.; Sparke, L. S.: *Pattern speeds in barred spiral galaxies* 1988, MNRAS, 231, 25

[18] Sellwood, J. A.: *Multiple Patterns in Spiral and Barred Galaxies* 1993, PASP, 105, 648

[19] Springel, V.; Yoshida, N.; White, S. D. M.: *GADGET: a code for collisionless and gasdynamical cosmological simulations* 2001, NewA, 6, 79

[20] Toomre, A.: *On the gravitational stability of a disk of stars* 1964, ApJ, 139, 1217

[21] Tremaine, S.; Weinberg, M. D.: *A kinematic method for measuring pattern speed of barred galaxies* 1984, ApJ, 282, 5T

[22] Weinberg, M. D.: *Evolution of barred galaxies by dynamical friction* 1985, MNRAS, 213, 451

[23] Yuan, C.: *Application of the Density-Wave Theory to the Spiral Structure of the Milky way System. I. Systematic Motion of Neutral Hydrogen* 1969, ApJ, 158, 871

[24] Yuan, C.: *Application of the Density-Wave Theory to the Spiral Structure of the Milky way System. II. Migration of Stars* 1969, ApJ, 158, 889

[25] Zimmer, P.; Rand, R. J.; McGraw, J. T.: *The Pattern Speeds of M51, M83, and NGC 6946 Using CO and the Tremaine-Weinberg Method* 2004, ApJ, 607, 285